

Implicit Dual-domain Convolutional Network for Robust Color Image Compression Artifact Reduction

Bolun Zheng, Yaowu Chen, and Xiang Tian, Fan Zhou, Xuesong Liu

1

Abstract—Several dual-domain convolutional neural network-based methods show outstanding performance in reducing image compression artifacts. However, they suffer from handling color images because the compression processes for gray-scale and color images are completely different. Moreover, these methods train a specific model for each compression quality and require multiple models to achieve different compression qualities. To address these problems, we proposed an implicit dual-domain convolutional network (IDCN) with the pixel position labeling map and the quantization tables as inputs. Specifically, we proposed an extractor-corrector framework-based dual-domain correction unit (DRU) as the basic component to formulate the IDCN. A dense block was introduced to improve the performance of extractor in DRU. The implicit dual-domain translation allows the IDCN to handle color images with the discrete cosine transform (DCT)-domain priors. A flexible version of IDCN (IDCN-f) was developed to handle a wide range of compression qualities. Experiments for both objective and subjective evaluations on benchmark datasets show that IDCN is superior to the state-of-the-art methods and IDCN-f exhibits excellent abilities to handle a wide range of compression qualities with little performance sacrifice and demonstrates great potential for practical applications.

Index Terms—JPEG Deblocking, Dual-domain Correction, Dense Connection, Pixel Labeling, Dilated Convolution

This Project is supported by Fundamental Research Funds for the Central Universities, China.

B. Zheng is with the Institute of Advanced Digital Technology and Instrument, Zhejiang University, Hangzhou 310027, China (e-mail: zhengbolun1024@163.com).

Y. Chen is with the State Key Laboratory of Industrial Control Technology, Zhejiang University, and also with the Embedded System Engineering Research Center, Ministry of Education of China, Zhejiang University, Hangzhou 310027, China (e-mail: yaowuchen@zju.edu.cn).

X. Tian is with the Institute of Advanced Digital Technology and Instrument, Zhejiang University, and is also with the Zhejiang Provincial Key Laboratory for Network Multimedia Technologies, Hangzhou 310027, China (e-mail: tianx@mail.bme.zju.edu.cn).

F. Zhou is with the Institute of Advanced Digital Technology and Instrument, Zhejiang University, and is also with the Zhejiang Provincial Key Laboratory for Network Multimedia Technologies, Hangzhou 310027, China

X. Liu is with the Institute of Advanced Digital Technology and Instrument, Zhejiang University, and is also with the Zhejiang Provincial Key Laboratory for Network Multimedia Technologies, Hangzhou 310027, China (e-mail:

I. INTRODUCTION

LOSSY image compression algorithms use the information redundancy of image patches to achieve the high compression ratio with desirable image qualities. Because the human eye is not sensitive to high-frequency information, most lossy image compression methods are implemented by quantization or approximation on the frequency domain. However, as the compression ratio increases, the artifacts introduced by the severe degradation of high-frequency information significantly reduce the quality of visual experience. JPEG is a representative lossy compression standard and widely used globally. JPEG compression standard divides the image into 8×8 patches and performs discrete cosine transform (DCT) on each patch. Then, the DCT coefficients are quantized and encoded into bit streams.

Studies of the reduction in image compression artifacts have recently been conducted and validated based on the JPEG compression standards. Traditional filter-based algorithms [1], [2] focus on general image denoising and play a role in image compression artifact reduction. Machine learning-based methods [3], [4], [5], [6] are more engaged in the specific image compression artifact reduction and present promising performance in both subjective and objective evaluations. These methods learn nonlinear mapping from the compressed image to the original image. Chen et al [4] trained nonlinear reaction diffusion models for image denoising and JPEG deblocking. Inspired by SRCNN [7], Dong et al. [5] first introduced a deep neural network (DNN) and built a four-layer full convolutional neural network (CNN) for compression artifact reduction, namely ARCNN. Previous studies on cascaded CNNs (CAS-CNNs) [8] and dual-domain multi-scale CNNs (DMCNNs) [9] imported MCNNs and learned large-scale features to remove the large-scale artifacts. Because JPEG compression artifacts are radically caused by the lossy quantization of DCT coefficients, Liu et al. [10] proposed a dual-domain image dictionary to recover the compressed images from both the pixel domain and the DCT domain. As DCT is a linear transformation that can be easily rewritten in a convolutional pattern, Guo et al. [11] proposed a dual-domain convolutional network (DDCN) and improved the performance on gray-scale images.

Despite their high performance on gray-scale images, DCT domain-based methods typically suffer from handling color images for two main reasons. First, because the whole network is a highly nonlinear system, simple linear operations on input

images would lead to unpredictable nonlinear outputs. In other words, using methods developed for gray-scale images to recover color images by restoring each color channel separately would lead to chromatic aberrations (Fig. 1). Second, because the compression algorithm for the luminance channel differs from that for the two chrominance channels, using a single model trained for the luminance channel to recover two chrominance channels would produce undesired results. However, for restoring color images compressed by JPEG, although pixel-domain learning methods can easily learn the correlations between each color channel, it is difficult to directly introduce the DCT-domain priors.

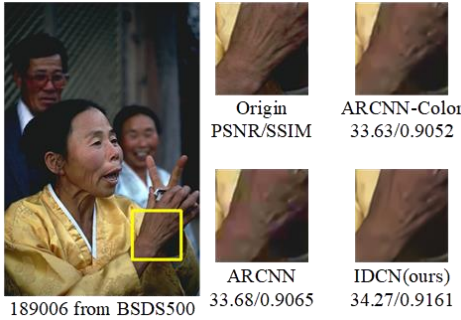


Fig. 1. Comparison between methods for gray-scale and color images. Here, ARCNN-Color refers to the ARCNN trained on color images.

The mapping relationship between the compression quality factor and the quantization coefficient can be expressed as

$$\varepsilon = \begin{cases} 200 + 50q & q \in \mathbb{N}^{(50,100)} \\ \frac{5000}{q} & q \in \mathbb{N}^{[1,50]} \end{cases} \quad (1)$$

$$Q^q = \mathfrak{R}\left(\frac{\varepsilon Q}{100}\right) \quad (2)$$

where q is the compression quality factor, Q is the base quantization coefficient table, Q^q is the quantization coefficient table with quality factor q , and \mathfrak{R} is the rounding operation. When q reaches a relatively low range, a slight change in q leads to a great change in Q^q . Thus, the performance of recovering DCT coefficients based on the prior of quantization coefficients severely declines when q of the recovered image mismatches the pre-trained model's q .

To address these problems, we propose a method to reduce high-quality color image compression artifacts by developing an implicit dual-domain convolutional network (IDCN) to implicitly utilize both pixel-domain features and DCT-domain priors. The main contributions of our work are summarized as follows:

- 1) We propose a unified architecture called IDCN to learn dual-domain corrections for the reduction in color image compression artifacts. To overcome the limitations of DCT, IDCN directly estimates the DCT-domain losses without DCT to build a color-to-color network.
- 2) We propose an extractor-corrector framework to construct generalized residual connection and develop the

dual-domain correction unit (DCU) based on this framework.

- 3) We introduce dilated convolution layers in the extractor of DCU to enlarge the receptive field, which shows great performance to remove wide-range distortions.
- 4) We propose a position labeling map to label the position of each pixel in the entire image and concatenate the position labeling map to the input image so that the network can utilize the position information to refine the compressed image.
- 5) We propose a flexible IDCN (IDCN-f) for robust color image compression artifact reduction. IDCN-f exhibits great performance in handling a wide range of compression qualities with one model weight.

II. RELATED WORK

Several CNN-based methods present promising potential to solve the image compression artifact reduction problem. In this section, we briefly review and discuss the methods relevant to this work.

Because the human eye is more sensitive to luminance than chrominance, early CNN-based methods focus on recovering the luminance channel of a JPEG compressed color image or only a gray-scale image. Dong et al. [5] first proposed a deep learning based method (ARCNN) for image compression artifact reduction. ARCNN is composed of four convolution layers: functions of these layers can be defined as feature extraction, feature enhancement, mapping, and reconstruction. However, as the network goes deeper, the function of each convolution layer is increasingly fused. Guo et al. [11] introduced a dual-domain learning architecture and built a 30-convolutional-layer network (DDCN) to utilize both the pixel-domain features and DCT-domain priors. DDCN consists of three branches: DCT-domain, pixel-domain, and aggregation, each containing 10 convolution layers. The DCT-domain branch replaces DCT and inverse DCT (iDCT) by equivalent convolution operations and quantization rectification is accomplished before the iDCT operation. Although dense DCT and iDCT convolution can utilize more redundant information from surrounding image patches to correct the DCT coefficients of the 8×8 image patches, it may also mislead the corrections for those middle image patches between the adjacent 8×8 image patches. Inspired by the success of CNN for single-image super resolution (SR), Cavigelli et al. [8] translated the compression artifact reduction problem to the super resolution problem and introduced stepped convolution layers and deconvolution [12] layers (also known as up-sampling layers) to build a cascaded convolutional network (CAS-CNN). CAS-CNN introduced a multi-scale loss function to restore the compressed image in a different scale. Multi-scale loss can enlarge the gradients for the bottom layers to update the learnable weights and learn large-scale features to recover the details. However, because the proportion of larger-scale feature maps is too low, the benefits from the multi-scale learning are limited. Noticing the merits of DDCN and CAS-CNN, Zhang et al. [9] proposed a DMCNN. They adopted the dual-domain framework and multi-scale loss and introduced dilated convolution layers to enlarge the receptive

fields for the removal of banding effects. Recently, Zheng et al. [13] further improved the CNN model by redefining the entire network as a combination of a feature encoder, a nonlinear feature mapper, and a feature decoder. Realizing the importance of the correlation of each color channel, they constructed a scalable convolutional network, S-Net, to learn a nonlinear mapping for color JPEG compressed image restoration. Unlike multi-scale losses calculated in different scales, S-Net formulates a greedy loss architecture (GLA) to maximize the performance of each convolutional unit at the original scale. They proved that the greedy theory-based training strategy would not suffer from local optimization and most subnetworks show better performance than normally trained networks under the same conditions.

Huang et al. [14] proposed DenseNet to ensure the maximum information flow between any layers within the same block and achieved state-of-the-art performance in high-level computer vision tasks. Following DenseNet, several low-level computer vision algorithms such as SRDenseNet [15], MemNet [16], and DCPDN [17] introduced dense connections and achieved impressive performance in respective fields.

All these methods of reduction in image compression artifacts showed significant improvement over conventional filter-based methods. However, none of them could effectively process the color images with DCT-domain priors. To address this problem, we propose an IDCN to represent the DCT-domain priors in the pixel-domain and fuse the corrections from both the DCT domain and the pixel domain. The details of IDCN are presented in Section III.

III. IMPLICIT DUAL-DOMAIN CONVOLUTION NETWORK

A. Implicit Translation from DCT-domain to Pixel-domain

A major obstacle to applying DCT-domain-based methods to color image processing is that the compressing operation for luminance channels is completely different from that for chrominance channels. First, chrominance channels should be downsampled by a factor of 2 before DCT, whereas luminance channels do not need downsampling. Second, the quantization table for luminance channels is different from that for chrominance channels. Conventional DCT-domain-based methods directly recover the DCT coefficients, which is difficult to be implemented in color images.

JPEG compression works on YCbCr mode images. The relationship between the YCbCr color space and the RGB color space can be expressed as

$$\begin{cases} R = 1.164(Y - 16) + 1.596(Cr - 128) \\ G = 1.164(Y - 16) - 0.392(Cb - 128) - 0.813(Cr - 128) \\ B = 1.164 * (Y - 16) + 2.017(Cb - 128) \end{cases} \quad (3)$$

where Y , Cb , and Cr denote the luminance channel and two chrominance channels, respectively, and R , G , and B denote the red, green, and blue channels, respectively. Therefore, we can easily calculate the RGB loss $\delta_{R,G,B}$ caused by JPEG compression:

$$\begin{aligned} \delta_{R,G,B} = & \left(\frac{\partial R}{\partial Y}, \frac{\partial G}{\partial Y}, \frac{\partial B}{\partial Y} \right) \delta_Y + \left(\frac{\partial R}{\partial Cb}, \frac{\partial G}{\partial Cb}, \frac{\partial B}{\partial Cb} \right) \delta_{Cb} \\ & + \left(\frac{\partial R}{\partial Cr}, \frac{\partial G}{\partial Cr}, \frac{\partial B}{\partial Cr} \right) \delta_{Cr} \end{aligned} \quad (4)$$

where δ_Y , δ_{Cb} , and δ_{Cr} denote the Y channel loss, Cb channel loss, and Cr channel loss caused by JPEG compression, respectively.

The losses caused by JPEG compression are mainly from the quantization operations on DCT coefficients. Considering Θ as an 8×8 DCT coefficient matrix and Θ^* as the quantized result of Θ , we can define Θ as

$$\Theta = \Theta^* + \delta_{\Theta} \quad (5)$$

where δ_{Θ} denotes the quantization loss. δ_{Θ} can be expressed as

$$\delta_{\Theta} = \mathcal{G} * Q^q \quad (6)$$

where $*$ denotes the element-wise multiplication and \mathcal{G} is the relative quantization loss, which is an 8×8 matrix and satisfies

$$-0.5 < \mathcal{G}_i < 0.5 \quad \forall \mathcal{G}_i \in \mathcal{G} \quad (7)$$

For an 8×8 image patch, the subchannel loss δ_s , $s \in \{Y, Cb, Cr\}$ in the YCbCr color space caused by the quantization of DCT coefficients can be written as

$$\begin{aligned} \delta_{s,i,j} &= \kappa(\Theta)_{i,j} - \kappa(\Theta^*)_{i,j} = \kappa(\delta_{\Theta})_{i,j}, i, j \in \mathbb{N}^{[0,7]} \\ &= \kappa(\mathcal{G} * Q^q)_{i,j} \\ &= \sum_{u=0}^7 \sum_{v=0}^7 \alpha(u)\alpha(v)\mathcal{G}_{u,v}Q_{u,v}^q f(i, j, u, v) \\ &= \mathcal{G} * \xi(Q^q, i, j) \end{aligned} \quad (8)$$

$$\left\{ \begin{aligned} \xi(Q^q, i, j)_{u,v} &= \alpha(u)\alpha(v)Q_{u,v}^q f(i, j, u, v) \quad u, v \in \mathbb{N}^{[0,7]} \\ \alpha(u) &= \sqrt{\frac{1}{8}} \quad u = 0 \\ \alpha(u) &= \sqrt{\frac{2}{8}} \quad u > 0 \end{aligned} \right. \quad (9)$$

$$f(i, j, u, v) = \cos \frac{(2i+1)u\pi}{16} \cos \frac{(2j+1)v\pi}{16} \quad (10)$$

where i and j denote the horizontal and vertical coordinates in the 8×8 image patch and κ denotes the iDCT operation. When δ_s , \mathcal{G} , and Q^q are reshaped into a $1 \times 1 \times 64$ vector, (8) can be rewritten as

$$\delta_s = \mathcal{G} * \xi_{1 \times 1}^*(Q^q) \quad (11)$$

$$\xi_{1 \times 1}^*(Q^q)_{8j+i} = \xi(Q^q)_{i,j} \quad (12)$$

where ξ^* is a $1 \times 1 \times 64 \times 64$ 2D convolution kernel. Therefore, we can use a 2D convolution to translate the DCT-domain loss to the pixel-domain loss in the YCbCr color space so that the element-wise operation in (6) can be avoided; this will reduce the calculations by approximately 40%. If we ignore the loss from the downsampling operation on chrominance channels, δ_Y , δ_{Cb} , and δ_{Cr} in (4) can be rewritten as

$$\delta_\chi = \mathcal{G}_\chi * \xi^*(Q_\chi^q), \chi \in \{Y, Cb, Cr\} \quad (13)$$

The quantization table of the Cb channel is the same as that of Cr ; thus, $Q_{Cr}^q = Q_{Cb}^q = Q_C^q$.

Estimating \mathcal{G}_Y , \mathcal{G}_{Cb} , and \mathcal{G}_{Cr} from the compressed image is a highly nonlinear task, which can always be handled in the pixel-feature domain and the estimated losses calculated from \mathcal{G}_Y , \mathcal{G}_{Cb} , and \mathcal{G}_{Cr} are in the YCbCr color space. Although we can translate the losses into the RGB color space by simple linear operations, we would rather translate the estimated loss back to the pixel-feature domain for two main reasons. First, the estimation task is handled in the feature-domain; this translation can keep the integrality of the whole nonlinear operation so that we can easily introduce skip connections to construct a deeper network. Second, for a specific pixel location in the image, the estimated δ_χ is a $1 \times 1 \times 64$ vector and it represents an 8×8 image patch, i.e., δ_χ of the locations in the same 8×8 stepped patch would be close to each other and the blocking effect probably exists in δ_χ . This translation can help to avoid the block effect of the deviation of δ_χ . Because this translation is operated from the pixel-feature domain to the pixel-feature domain and utilizes the prior from the DCT-domain, we call this translation an implicit dual-domain translation.

B. Position Labeling

Because most elements in the quantization table are different

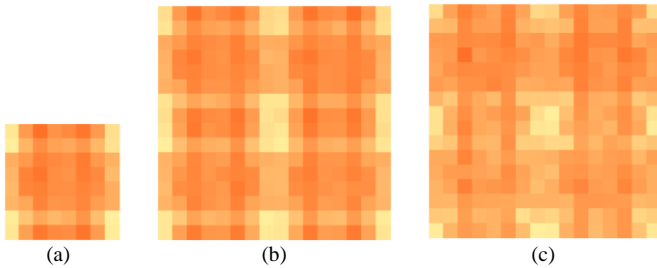


Fig. 2. Standard deviation maps with $q = 20$. (a) Patch size is 8, WIN143. (b) Patch size is 16, WIN143. (c) Patch size is 16, 200 testing images of BSDS500.

from each other and the loss of DCT coefficients at different positions leads to different losses in the RGB color space, the RGB color space loss caused by the quantization of different pixels in an 8×8 patch would probably be different from each other. We conducted an experiment on the DIV2K dataset to validate our assumption. As the chrominance channels are downsampled before DCT and quantization operations, we separated the luminance channel from the image and sliced the luminance channel into 8×8 patches in accordance with the JPEG image. Then, we calculated the standard deviation of the

difference between the original image and the JPEG compressed image at different positions. The result is shown in Fig. 2(a). The standard deviations of the elements around the corners are larger than in the middle. To further support this conclusion, we increased the patch size to 16 and kept the moving step unchanged. The standard deviation map (Fig. 2(b)) varies in cycles of 8×8 , which is the same as the field of the DCT patch. We also conducted this experiment on other public image datasets (Fig. 2(c)). Although the ranges of standard deviation are different, the regularity of distributions is close. If we expand this result to the entire RGB color space, the minimum period of the standard deviation should be 16×16 .

Based on this conclusion, it is necessary to consider the position of the pixels. The deviation is introduced by quantization in the DCT-domain. Based on the randomness of the quantization operation, we can use a zero-mean Gaussian distribution to simply describe this deviation. Thus, the deviation distribution at a specific position could be defined as

$$\psi_{i,j} = \mathbb{N}(0, \sigma_{i,j}) \quad i, j \in \mathbb{N}^{[0,7]} \quad (14)$$

where \mathbb{N} denotes the Gaussian distribution and $\sigma_{i,j}$ denotes the standard deviation at position (i, j) . Inspired by FFDNet [18], we used the standard deviation to label the pixel position and we called this standard deviation map a “label map.” The label map has the same size as the input image and is defined as

$$L^\chi(x, y) = \sigma_{\text{mod}(x,\omega), \text{mod}(y,\omega)}^\chi, \chi \in \{R, G, B\} \quad (15)$$

where L denotes the label map and ω denotes the minimum period of standard deviation in each axis. For color images, the channel size of the label map is 3 and $\omega = 16$ (Fig. 3).

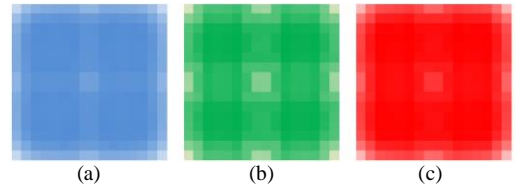


Fig. 3. Standard deviation maps with $q = 20$ on DIV2K dataset. (a) B channel. (b) G channel. (c) R channel.

C. Architecture

Fig. 4 illustrates the architecture of IDCN, which mainly consists of three parts: feature encoder (FE), correction baseline (CB), and feature decoder (FD). We denote I_{in} and I_{out} as the input and output of IDCN. Specifically, based on the previous studies, the batch-normalization [19] layer was not considered. FE takes two convolution layers to encode the input from the pixel domain to the pixel-feature domain and each convolution layer is linked to a ReLU [20] layer. The first 5×5 convolution layer and the ReLU layer extract features f_0 from I_{in} .

$$f_0 = \text{Max}(\mathbb{C}_{FE}(I_{in}), 0) \quad (16)$$

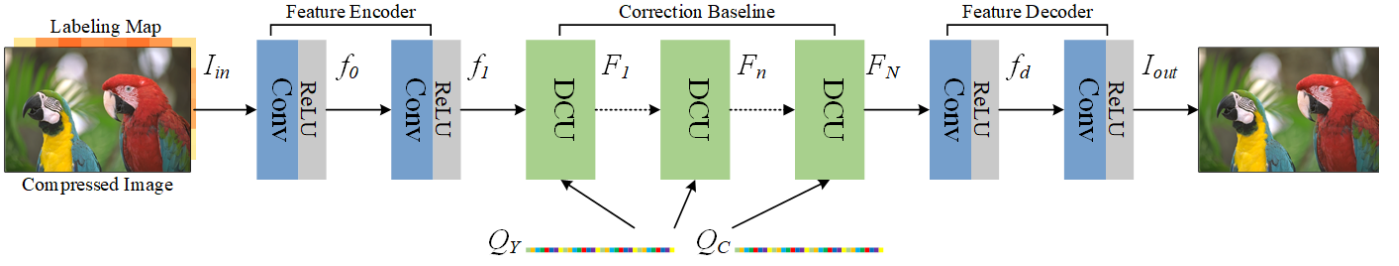


Fig. 4. Architecture of our proposed implicit dual-domain convolutional network (IDCN)

where \mathbb{C}_{FE1} denotes the convolution operation of the first convolution layer of FE. The second 3×3 convolution layer and the ReLU layer then further enhance f_0 to obtain f_1 for feature-domain corrections.

$$f_1 = \text{Max}(\mathbb{C}_{FE2}(f_0), 0) \quad (17)$$

where \mathbb{C}_{FE2} denotes the convolution operation of the second convolution layer of FE. f_1 is then used as an input to CB, which consists of a series of DCUs. Assuming that CB contains N DCUs, the output F_n of the n -th DCU can be expressed as

$$F_n = \mathfrak{U}_{CB,n}(F_{n-1}) = \mathfrak{U}_{CB,n}(\mathfrak{U}_{CB,n-1}(\dots(\mathfrak{U}_{CB,1}(f_1))\dots)) \quad (18)$$

where $\mathfrak{U}_{CB,n}$ denotes the dual-domain correction operation of the n -th DCU. The details on DCU are provided in Section III.D. The corrected feature (F_n) output by CB is then sent to FD. The FD takes two convolution layers to translate F_n to final output I_{out} . The first 3×3 convolution layer and the ReLU layer preprocess the corrected features (F_n) to decodable features (f_d).

$$f_d = \text{Max}(\mathbb{C}_{FD1}(F_n), 0) \quad (19)$$

where \mathbb{C}_{FD1} denotes the convolution operation of the first convolution layer in FD. The second 5×5 convolution layer then translates f_d to I_{out} .

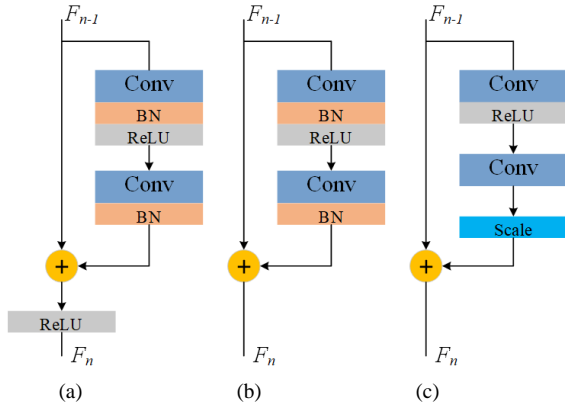


Fig. 5. Comparison of residual connections in original ResNet, SRResNet, and EDSR. (a) Original ResNet. (b) SRResNet. (c) EDSR.

$$I_{out} = \mathbb{C}_{FD2}(f_d) \quad (20)$$

where \mathbb{C}_{FD2} denotes the convolution operation of the second convolution layer in FD. In our IDCN, \mathbb{C}_{FE1} , \mathbb{C}_{FE2} , and \mathbb{C}_{FD1} have the same number of filters and \mathbb{C}_{FD2} have three filters as we output the color images.

D. Dual-domain Correction Unit

The DCU is designed based on residual learning and on the results presented in Section III.A. We compared several versions of residual connections (Fig. 5). Fig. 5 (a) shows the original residual connection in ResNet [21]. SRResNet [22] (Fig. 5(b)) modified the original residual connection by removing the outside ReLU layer for single-image super resolution. The enhanced deep super-resolution network (EDSR) [23] (Fig. 5(c)) further improved the residual connection in SRResNet by removing the batch-normalization layers and concatenating the scaling layer to the residual branch to avoid gradient explosion. The residual branch can be regarded as an extractor-corrector framework. For example, in Fig. 5(c), the first convolution layer and the ReLU layer can be regarded as a simple feature extractor and the second convolution layer and the scaling layer as a simple corrector.

In our DCU, we reconstructed the feature extractor by importing the dense block and the transition block. We also reconstructed the corrector by introducing dual correction branches, DCT-domain and pixel-domain, so that our DCU can make the corrections through both pixel and DCT domains. The structure of DCU is shown in Fig. 6. The two correction branches share the same feature extractor, shared feature extractor (SFE). Let F_{n-1} and F_n be the input and output of the n -th DCU. SFE takes F_{n-1} as the input and outputs the basic features F_g for the DCT-domain branch to estimate DCT-domain correction δ_{DCT} and pixel-domain correction δ_{Pixel} . Then, we used a residual connection to connect F_{n-1} , δ_{DCT} , and δ_{Pixel} together to obtain F_n :

$$F_n = F_{n-1} + \delta_{DCT} + \delta_{Pixel} \quad (21)$$

SFE consists of a dense block and a transition block. The dense block is a group of densely connected 3×3 convolution layers to extract high-dimensional features. Transition block is a 1×1 convolution layer with the ReLU activation layer to compress the high-dimensional features to low-dimensional

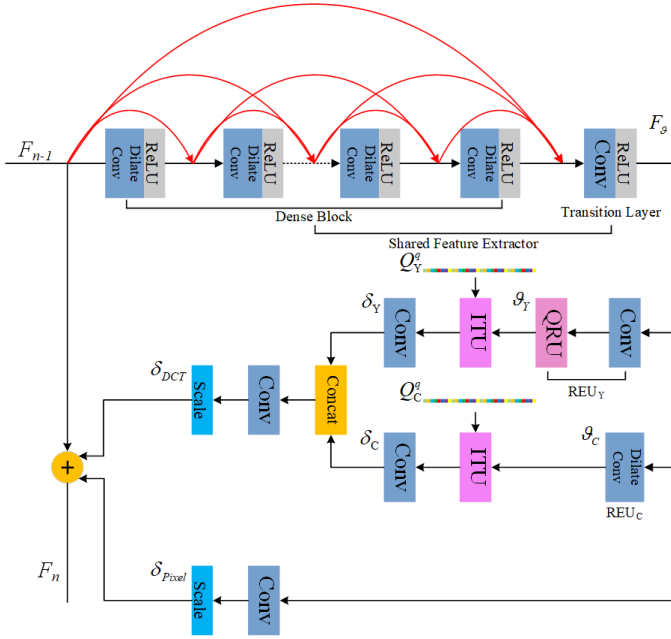


Fig. 6. Architecture of our proposed dual-domain correction unit.

features. We assumed that SFE contains L convolution layers and the growth is K . The number of filters of the first convolution layer in the dense block was set to $2K$. Then, the number of filters of the remaining $L-2$ convolution layers was set to K . The outputs of the first $L-1$ convolution layers were concatenated together to be sent to the transition block. Moreover, we adopted the receptive field theory in DMCNN and introduced dilated convolution [24] to enlarge the receptive field of feature extractors. For the first $L-1$ densely connected layers, the first half of the layers were normal convolution layers (dilation rate was 1) and then the dilation rate was increased by 1 for each stacked convolution layer.

In the DCT-domain branch, relative quantization loss estimating unit (REU) takes F_g as input and uses a 3×3 convolution layer and quantization rectified unit (QRU) to estimate the relative quantization loss \mathcal{G} in a specific channel of Y , Cr , and Cb . Here, QRU is a simple constraint layer to let \mathcal{G} satisfy (7). One REU estimates the loss from a channel of Y , Cb , and Cr . However, taking three REUs to estimate \mathcal{G}_Y , \mathcal{G}_{Cb} , and \mathcal{G}_{Cr} would introduce too many learnable parameters, which would increase the computation consumption and make the network difficult to converge. Because Y channel is a major channel for human visual sense and Cb and Cr channels share the same quantization table, we use one REU, REU_Y , to estimate \mathcal{G}_Y and another one, REU_C , to estimate the integrated chrominance loss \mathcal{G}_C . Because REU_C estimates the integrated loss from both Cr and Cb channels, the constraints based on (7) do not work on \mathcal{G}_C ; thus, QRU is not included in REU_C . Moreover, because the two chrominance channels are compressed in the DCT domain after the 2×2 downsampling operation, we introduced a 3×3 dilated convolution layer with a dilation rate of 2 for REU_C , whereas REU_Y is a normal 3×3 convolution layer. Then, the implicit translation units (ITUs) generated by Q_Y^g and Q_C^g translate \mathcal{G}_Y and \mathcal{G}_C to the

luminance loss δ_Y and chrominance loss δ_C , respectively, based on (8–13). Finally, we concatenated δ_Y and δ_C together and used a 3×3 convolution layer to fuse them to obtain the final pixel-feature domain correction of DCT-domain branch δ_{DCT} . In the pixel-domain branch, we used a 3×3 convolution layer as a simple corrector to obtain the pixel-feature domain correction of pixel-domain branch δ_{Pixel} . To avoid gradient explosion, we introduced a scale layer in EDSR to scale both δ_{DCT} and δ_{Pixel} . The scaling rate was set to 0.1.

IV. EXPERIMENTAL EVALUATION

A. Implementation Details

Network Settings. In the proposed IDCN, CB has $N=8$ DCUs and each DCU has the same structure, $K=64$ and $L=8$. Except the second convolution layer in FD, all the other convolution layers in FE and FD and all the trainable convolution layers in two correction branches have $B=64$ filters. Specifically, the number of filters of the convolution layers in REU is fixed to 64 because the relative quantization losses of 64 DCT coefficients are output.

Datasets and Metrics. The DIV2K [25] dataset has been recently released for single-image SR. DIV2K consists of 1000 high-quality (2K resolution) images (800 training images, 100 validation images, and 100 test images). Because the test images are prepared for single-image SR competition and the ground truth has not been released, these images were not included in our experiment. We trained our models on 900 images including 800 training images and 100 validation images and conducted validation and testing on other three standard datasets: BSDS500 [26], LIVE1 [27], and WIN143 [13]. We used half of 100 validation images of BSDS500 for validation during training. For testing, quantitative evaluations were conducted on 200 test images of BSDS500, 29 images of LIVE1, and 143 images of WIN143.

For quantitative evaluations, we used standard MATLAB library functions. The objective performance indicators peak signal-to-noise ratio (PSNR) and structural similarity index (SSIM) were measured with only the luminance channels considered.

Training Settings. All the model weights of the proposed IDCN were trained using the same training settings. We regarded the L2 loss as the loss function. We used Adam as our training optimizer with reference parameters. The learning rate was set to 10^{-4} for all layers. If the decrease in the validation loss is lower than 0.001 dB for three consecutive epochs, the learning rate is divided by 5. If the learning rate is lower than 10^{-6} , it is set to 10^{-6} and kept unchanged. If the learning rate reaches 10^{-6} and the decrease in the validation loss is lower than 0.001 dB for consecutive five epochs, the training is stopped. Referring to the settings in DMCNN, we randomly cropped 43×43 RGB patches with the batch size of 16 as the input and then enlarged the patch size to 96×96 . The batch size is cut to 8 when the learning rate reaches 10^{-6} . For patch inputs with a size of 43×43 , 5000 batches constitute an epoch and for those with a size of 96×96 , 3000 batches constitute an epoch.

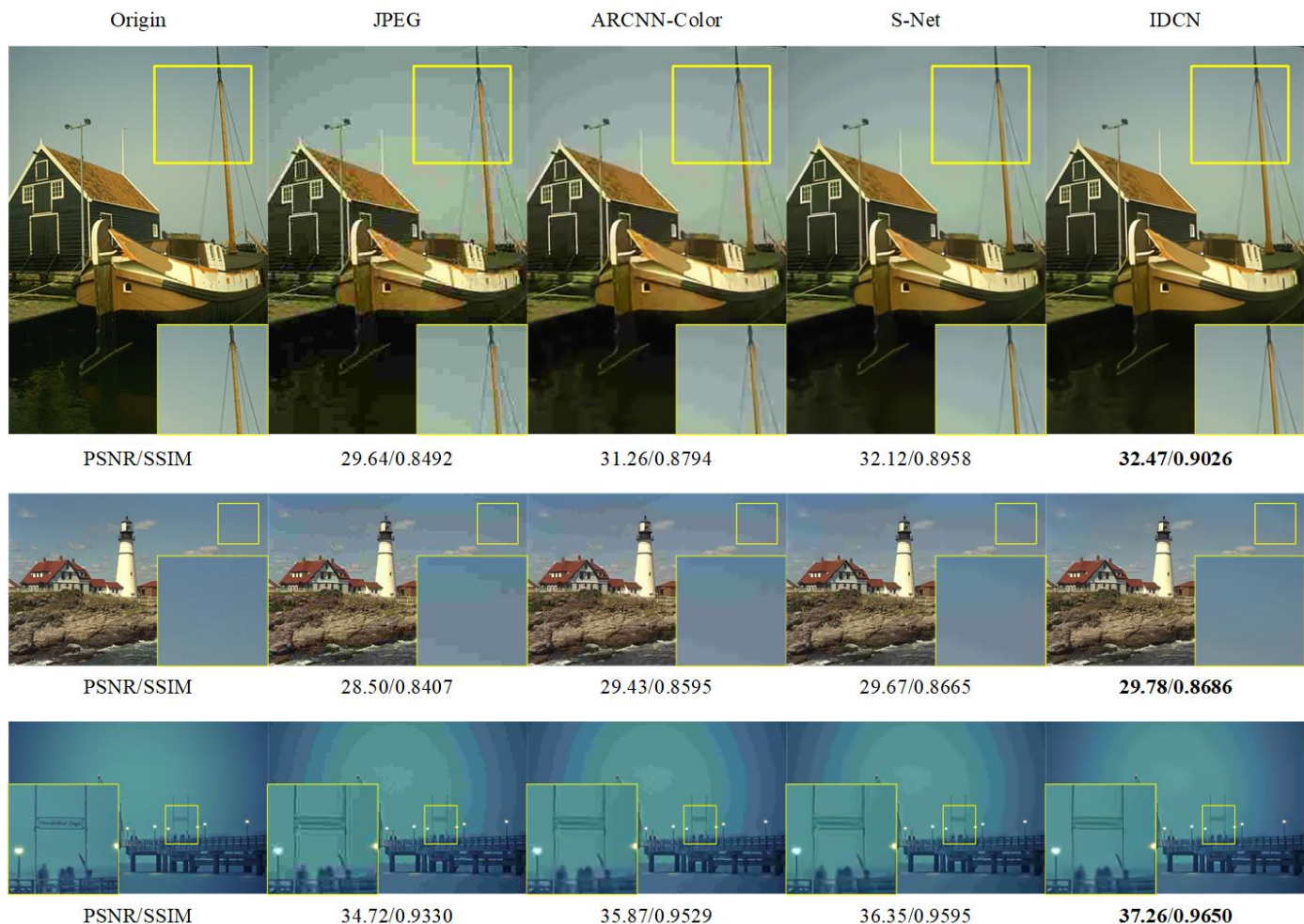


Fig. 7. Subjective evaluation with compression quality $q=10$. From top to bottom: 140088 from BSDS500, lighthouse2 from LIVE1, 005 from WIN143.

We implemented the IDCN using the Keras framework and Tensorflow backend. Training IDCN roughly takes seven days on a K80 GPU server for 100 epochs.

TABLE I
ABLATION INVESTIGATION OF POSITION LABELING (PL) AND MULTI-CHANNEL CORRECTION (MCC). WE OBSERVE THE BEST PERFORMANCE ON LIVE1 DATASET WITH COMPRESSION QUALITY $q=20$.

PL Options		MCC Options		PSNR (dB)
-N	-L	-FC	-SC	
√		√		31.91
	√	√		31.96
√			√	<u>32.00</u>
	√		√	<u>32.04</u>

B. Ablation Investigation

In this section, we investigate the effects of two optional items: position labeling (PL) and multi-channel correction (MCC). PL has three options: no position labeling (-N) and position labeling (-L). MCC has two options: full correction (-FC), and simple correction (-SC). Here, full correction refers to making corrections from Y, Cb, and Cr, and simple correction refers to making corrections from the luminance channel and combined chrominance channel. Table I shows the results of the ablation investigation of the effects of options on

PL and MCC. Four networks have the same network settings; $N=3$, $K=20$, $L=6$, and $B=64$. This investigation was conducted on LIVE1 with $q=20$ and the performance indicator is PSNR. Using -FC options may lead to worse results. Too many subbranches in the DCT-domain correction branch cannot further improve the performance but may scatter the loss back-propagation. Using -SC option instead can effectively simplify the network and make a significant improvement. Selecting -L option can also improve the performance by introducing pixel position information.

C. Subjective Comparison

For a subjective comparison, we focused on reducing the color image compression artifacts, not on the approaches to process gray-scale images. We compared IDCN with S-Net and ARCNN-Color, which is the color version of ARCNN trained by our research group. ARCNN-Color has the same structure as the original ARCNN, but the output channels of the reconstruction layer are changed to 3 in ARCNN-Color to output the color images. We trained ARCNN-Color on the DIV2K dataset and adopted the same training strategies as in ARCNN. Fig. 7 shows that IDCN produces more defined edges, whereas the block effects more or less exist in the results of S-Net and ARCNN-Color. Moreover, IDCN is more robust to

TABLE II
QUANTITATIVE COMPARISON ON LIVE1 AND 200 TESTING IMAGES OF BSDS500. AVERAGE PSNR/SSIM VALUES FOR COMPRESSION QUALITY $q=10$ AND 20. THE BEST RESULTS ARE HIGHLIGHTED.

Dataset	Quality	JPEG	ARCNN-Col or	CAS-CNN	DDCN	ARN	MemNet	DMCNN	S-Net	IDCN
LIVE1	20	30.62/0.8816	31.78/0.8985	31.70/0.895	-/-	31.34/0.8696	31.83/0.8846	32.09/0.905	32.26/0.9067	32.32/0.9077
	10	28.36/0.8116	29.49/0.8363	29.44/0.833	-/-	29.27/0.8077	29.45/0.8193	29.73/0.842	29.87/0.8467	29.99/0.8503
BSDS 500	20	30.61/0.8811	31.71/0.8986	-/-	31.88/0.8996	-/-	-/-	31.98/0.904	32.15/0.9047	32.22/0.9058
	10	28.39/0.8098	29.45/0.8338	-/-	29.59/0.8381	-/-	-/-	29.67/0.840	29.82/0.8440	29.94/0.8475

handle the wide-range color distortion, whereas the color band phenomenon cannot be totally removed by S-Net and ARCNN-Color. Generally, IDCN generates more visually pleasing results.

D. Objective Comparison

For an objective comparison, we used PSNR and SSIM as indicators to evaluate the performance of different methods.

TABLE III
EXTENDED QUANTITATIVE COMPARISON ON WIN143. AVERAGE PSNR/SSIM VALUES FOR COMPRESSION QUALITY $q=10$ AND 20. THE BEST RESULTS ARE HIGHLIGHTED.

Quality	JPEG	ARCNN-Col or	S-Net	IDCN
20	32.95/0.9033	34.08/0.9179	34.61/0.9250	34.74/0.9263
10	30.56/0.8432	31.76/0.8707	32.15/0.8795	32.46/0.8847

We measured PSNR and SSIM considering only the luminance channel and all the measurements were completed on the MATLAB platform. We compared IDCN with other state-of-the-art methods including ARCNN-Color [5], CAS-CNN [8], ARN [28], MemNet [16], S-Net [13], DMCNN [9], and DDCN [11]. Because DMCNN, DDCN, CAS-CNN, and MemNet do not provide the source code, the results were obtained from the original publications. Quantitative results on LIVE1 and BSDS500 testing sets are shown in Table II. IDCN exhibits a significant improvement on all datasets, compression qualities, and metrics compared to the other methods. As q becomes lower, the gap is further increased. To further demonstrate the generality and universality of IDCN, we conducted an expanded comparison on the WIN143 dataset with ARCNN-Color and S-Net. We followed the experimental settings in S-Net that uses bi-cubic interpolations to reduce the image size by half and we retrained S-Net for the evaluation of $q=10$. Quantitative results of the expanded comparisons are shown in Table III. IDCN outperforms all the other methods on all compression qualities and metrics.

E. Robust Compression Artifact Reduction

For image compression, especially in JPEG standards, the compression quality q is always known. We trained a flexible IDCN (IDCN-f) to handle the compressed images with different q . Because the labeling map is generated by statistical priority for different q , it is not convenient to calculate all the statistical priorities of different q values. We assume that IDCN-f is trained for compression qualities in $N^{[ql,qh]}$. We first calculate the labeling maps L_{ql} and L_{qh} of ql and qh , respectively, and the labeling map of q in $N^{[ql,qh]}$ is generated by

$$L_q = \frac{q-ql}{qh-ql} L_{qh} + \frac{qh-q}{qh-ql} L_{ql} \quad (22)$$

To cover the low compression quality, we trained IDCN-f in $N^{[5,20]}$. Quantitative results of IDCN-f on LIVE1 are shown in Table IV.

IDCN-f achieved high-performance levels for all q values. Although there is a slight performance degradation compared to the specifically trained IDCN models, IDCN-f exhibits better performance than most state-of-the-art methods. Fig. 8 shows the performance curves of IDCN-f and other specifically trained IDCN models, IDCN-10 and IDCN-20, in the compression quality range of $N^{[5,20]}$. Here, IDCN-10 and IDCN-20 refer to the IDCN model trained with compression qualities $q=10$ and 20, respectively. IDCN-f exhibits great robustness to handle variant compression qualities, whereas the specifically trained IDCN models cannot handle those mismatched compression qualities. Fig. 9 shows the subjective comparison on a section of the BSDS500 testing dataset. IDCN-20 obtained terrible results when handling lower compression qualities for both objective and subjective evaluations. Although IDCN-10 could obtain relatively better results than IDCN-20, the chromatic aberration and missing details remained. By contrast, IDCN-f could fix both chromatic aberration and texture details for a wide range of compression qualities.

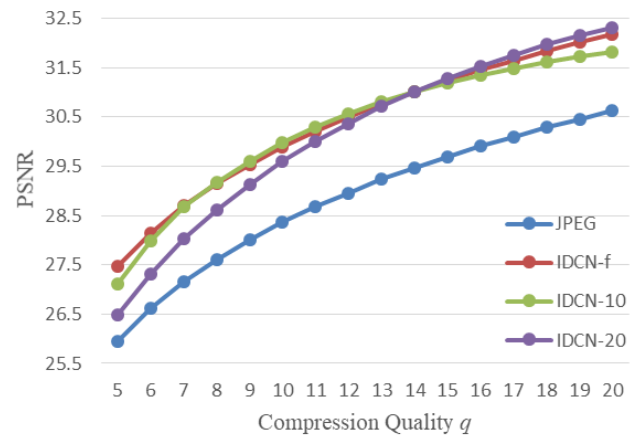


Fig. 8. Performance curves of JPEG, IDCN-f, IDCN-10, and IDCN-20. The averaged PSNR values are evaluated on LIVE1.

V. CONCLUSIONS

In this study, we proposed a novel network based on implicit dual-domain learning (IDCN) to reduce color image

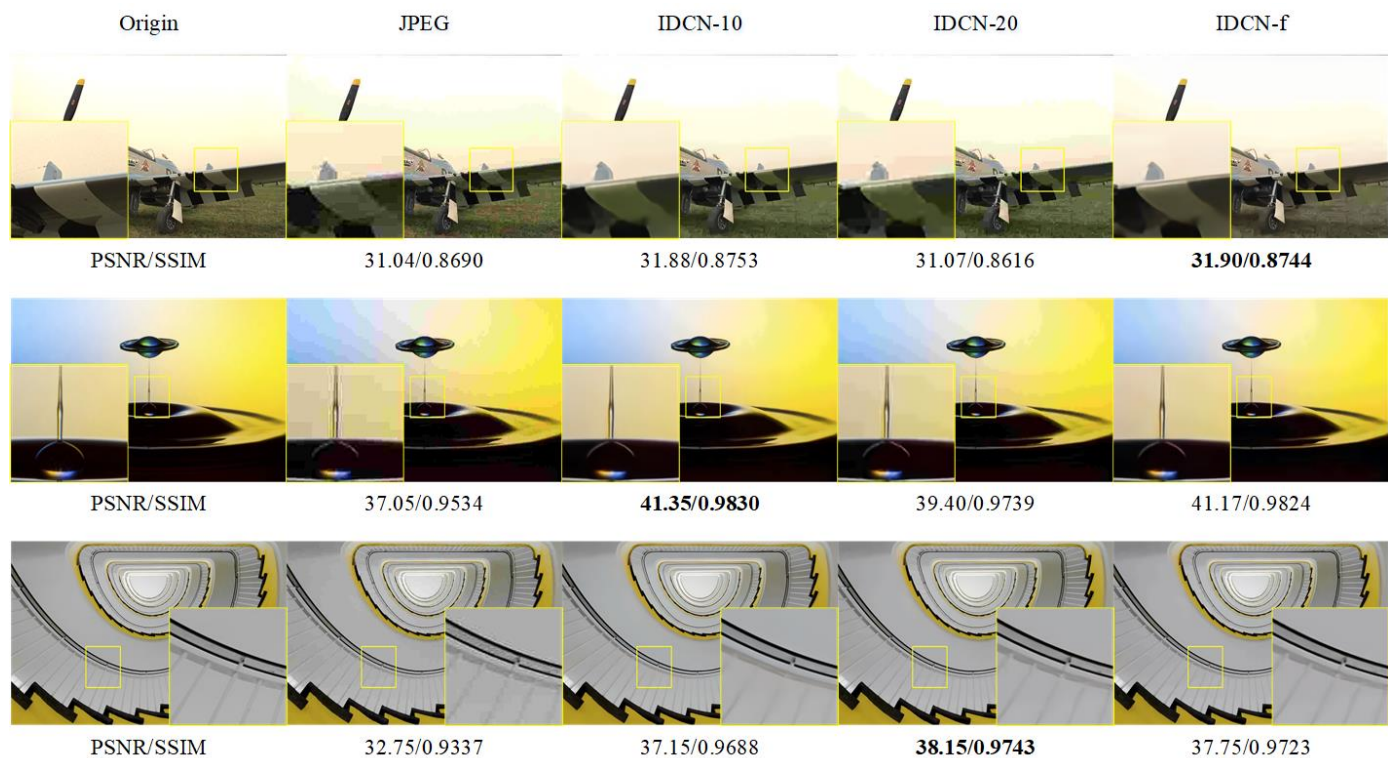


Fig. 9. Subjective evaluation for robust compression artifact reduction. From top to bottom: plane from LIVE1 and $q=7$, 024 from WIN143 and $q=10$, 038 from WIN143 and $q=20$.

compression artifacts. We first analyzed the structure of the conventional residual connections for low-level computer vision tasks and presented the extractor-corrector framework for constructing more generalized residual connections. Then, we constructed a correction unit based on this framework and introduced dense connections for the extractor and dual-domain correction for the corrector. Unlike conventional dual-domain learning methods that introduce DCT to enter the DCT-domain, the losses in the DCT-domain are directly estimated from the extracted features without DCT. DCU also benefits the larger receptive field from dilated convolution layers to obtain superior results in low-compression quality images. We compared IDCN with other state-of-the-art methods on both widely used evaluation datasets and the expanded WIN143 dataset. The objective and subjective evaluations demonstrate the superiority of IDCN over the other state-of-the-art methods. Moreover, the flexible version of IDCN named IDCN-f presents great performance to handle variable compression qualities in both subjective and objective evaluations. Therefore, IDCN-f has great potential for applications in practical compression artifact reduction efforts.

REFERENCES

- 1 Foi, A., Katkovnik, V., and Egiazarian, K.: 'Pointwise shape-adaptive DCT for high-quality denoising and deblocking of grayscale and color images', *IEEE Transactions on Image Processing*, 2007, 16, (5), pp. 1395-1411
- 2 Dabov, K., Foi, A., Katkovnik, V., and Egiazarian, K.: 'Image Denoising by Sparse 3-D Transform-Domain Collaborative Filtering', *IEEE Transactions on Image Processing*, 2007, 16, (8), pp. 2080-2095
- 3 Chang, H., Ng, M.K., and Zeng, T.: 'Reducing Artifacts in JPEG Decompression Via a Learned Dictionary', *IEEE Transactions on Signal Processing*, 2014, 62, (3), pp. 718-728
- 4 Chen, Y., Yu, W., and Pock, T.: 'On learning optimized reaction diffusion processes for effective image restoration', in Editor (Ed.) (Eds.): 'Book Learning optimized reaction diffusion processes for effective image restoration' (2015, edn.), pp. 5261-5269
- 5 Dong, C., Deng, Y., Chen, C.L., and Tang, X.: 'Compression Artifacts Reduction by a Deep Convolutional Network', in Editor (Ed.) (Eds.): 'Book Compression Artifacts Reduction by a Deep Convolutional Network' (2015, edn.), pp. 576-584
- 6 Svoboda, P., Hradis, M., Barina, D., and Zemcik, P.: 'Compression Artifacts Removal Using Convolutional Neural Networks', *Journal of Wscg*, 2016, 24, (2), pp. 63-72
- 7 Dong, C., Loy, C.C., He, K., and Tang, X.: 'Learning a deep convolutional network for image super-resolution', in Editor (Ed.) (Eds.): 'Book Learning a deep convolutional network for image super-resolution' (Springer, 2014, edn.), pp. 184-199
- 8 Cavigelli, L., Hager, P., and Benini, L.: 'CAS-CNN: A deep convolutional neural network for image compression artifact suppression', in Editor (Ed.) (Eds.): 'Book CAS-CNN: A deep convolutional neural network for image compression artifact suppression' (2017, edn.), pp. 752-759
- 9 Zhang, X., Yang, W., Hu, Y., and Liu, J.: 'DMCNN: Dual-Domain Multi-Scale Convolutional Neural Network for Compression Artifacts Removal', 2018
- 10 Liu, X., Wu, X., Zhou, J., and Zhao, D.: 'Data-driven sparsity-based restoration of JPEG-compressed images in dual transform-pixel domain', in Editor (Ed.) (Eds.): 'Book Data-driven sparsity-based restoration of JPEG-compressed images in dual transform-pixel domain' (2015, edn.), pp. 5171-5178
- 11 Guo, J., and Chao, H.: 'Building Dual-Domain Representations for Compression Artifacts Reduction', in Editor (Ed.) (Eds.): 'Book Building Dual-Domain Representations for Compression Artifacts Reduction' (2016, edn.), pp. 628-644
- 12 Noh, H., Hong, S., and Han, B.: 'Learning Deconvolution Network for Semantic Segmentation', international conference on computer vision, 2015, pp. 1520-1528
- 13 Zheng, B., Sun, R., Tian, X., and Chen, Y.: 'S-Net: a scalable convolutional neural network for JPEG compression artifact reduction', in Editor (Ed.) (Eds.): 'Book S-Net: a scalable convolutional neural network for JPEG compression artifact reduction' (SPIE, 2018, edn.), pp. 12
- 14 Huang, G., Liu, Z., Laurens, V.D.M., and Weinberger, K.Q.: 'Densely Connected Convolutional Networks', 2016, pp. 2261-2269

- 15 Tong, T., Li, G., Liu, X., and Gao, Q.: 'Image Super-Resolution Using Dense Skip Connections', in Editor (Ed.)^(Eds.): 'Book Image Super-Resolution Using Dense Skip Connections' (2017, edn.), pp. 4809-4817
- 16 Tai, Y., Yang, J., Liu, X., and Xu, C.: 'MemNet: A Persistent Memory Network for Image Restoration', in Editor (Ed.)^(Eds.): 'Book MemNet: A Persistent Memory Network for Image Restoration' (2017, edn.), pp. 4549-4557
- 17 Zhang, H., and Patel, V.M.: 'Densely Connected Pyramid Dehazing Network', 2018
- 18 Zhang, K., Zuo, W., and Zhang, L.: 'FFDNet: Toward a Fast and Flexible Solution for CNN based Image Denoising', IEEE Transactions on Image Processing, 2017, PP, (99), pp. 1-1
- 19 Ioffe, S., and Szegedy, C.: 'Batch normalization: Accelerating deep network training by reducing internal covariate shift', in Editor (Ed.)^(Eds.): 'Book Batch normalization: Accelerating deep network training by reducing internal covariate shift' (2015, edn.), pp. 448-456
- 20 Nair, V., and Hinton, G.E.: 'Rectified Linear Units Improve Restricted Boltzmann Machines', in Editor (Ed.)^(Eds.): 'Book Rectified Linear Units Improve Restricted Boltzmann Machines' (2010, edn.), pp. 807-814
- 21 He, K., Zhang, X., Ren, S., and Sun, J.: 'Deep Residual Learning for Image Recognition', in Editor (Ed.)^(Eds.): 'Book Deep Residual Learning for Image Recognition' (2016, edn.), pp. 770-778
- 22 Ledig, C., Theis, L., Huszár, F., Caballero, J., Cunningham, A., Acosta, A., Aitken, A., Tejani, A., Totz, J., and Wang, Z.: 'Photo-realistic single image super-resolution using a generative adversarial network', arXiv preprint, 2016
- 23 Lim, B., Son, S., Kim, H., Nah, S., and Lee, K.M.: 'Enhanced Deep Residual Networks for Single Image Super-Resolution', in Editor (Ed.)^(Eds.): 'Book Enhanced Deep Residual Networks for Single Image Super-Resolution' (2017, edn.), pp. 1132-1140
- 24 Yu, F., and Koltun, V.: 'Multi-scale context aggregation by dilated convolutions', arXiv preprint arXiv:1511.07122, 2015
- 25 Timofte, R., Lee, K.M., Wang, X., Tian, Y., Yu, K., Zhang, Y., Wu, S., Dong, C., Lin, L., and Qiao, Y.: 'NTIRE 2017 Challenge on Single Image Super-Resolution: Methods and Results', in Editor (Ed.)^(Eds.): 'Book NTIRE 2017 Challenge on Single Image Super-Resolution: Methods and Results' (2017, edn.), pp. 1110-1121
- 26 Arbelaez, P., Maire, M., Fowlkes, C., and Malik, J.: 'Contour Detection and Hierarchical Image Segmentation', IEEE Transactions on Pattern Analysis & machine Intelligence, 2011, 33, (5), pp. 898
- 27 Sheikh, H.R.: 'LIVE Image Quality Assessment Database', 2003
- 28 Zhang, Y., Sun, L., Yan, C., Ji, X., and Dai, Q.: 'Adaptive Residual Networks for High-Quality Image Restoration', IEEE Transactions on Image Processing, 2018, PP, (99), pp. 1-1